AJNR Am J Neuroradiol 25:1225–1233, August 2004

Neuronal and Glial Cell Populations in the Piriform Cortex Distinguished by Using an Approximation of *q*-Space Imaging after Status Epilepticus

Shawnee Eidt, Edward J. Kendall, and André Obenaus

BACKGROUND AND PURPOSE: **Temporal lobe epilepsy produces an injury cascade that includes neuronal loss and gliosis. The pilocarpine model reliably reproduces the symptoms of temporal lobe epilepsy and the resulting neuronal glial changes can be accurately depicted on diffusion-weighted images. The judicious choice of diffusion-encoding gradients can isolate multiple apparently isochromatic diffusing populations, but the assignment of these populations to specific tissue characteristics has been difficult. We sought to distinguish neuronal tissue from glial cell–infiltrated tissue by using signatures from unique spin populations obtained from an approximation of *q*-space imaging.**

METHODS: **Ten male Sprague-Dawley rats received pilocarpine injections to induce seizures. All animals underwent diffusion-weighted imaging at 12 hours, 24 hours, and 7 days. At least two animals were selected for histologic analysis at each imaging time point.**

RESULTS: **The results indicated that seizure-induced neurologic dysfunction may have been reflected in the emergence of new spin populations. In the piriform cortex–amygdala region of interest, the mean free diffusion path increased from 12 to 20 μm within 12 hours of seizure onset and persisted for at least 7 days. These results were temporally correlated with histologic evidence of necrotic changes.**

CONCLUSION: **Our results suggest that even incomplete sampling of *q* space can provide useful physiologic information.**

Temporal lobe epilepsy (TLE) produces an injury cascade that results in abnormality of the hippocampal formation, piriform cortex, and amygdaloid nuclei. Neuronal loss and gliosis in these limbic structures are hallmarks of TLE, with the hippocampus often being the most vulnerable area (1).

The rodent-based pilocarpine model of TLE produces sustained seizures mediated by excessive cholinergic stimulation. Injury is characteristically limited to electrically active regions of the forebrain and characterized by seizure-induced injury in the hippocampus, amygdala, thalamus, olfactory cortex, substantia nigra, and temporal cortices (2). Thus, the pilocarpine model produces changes similar to those associated with human TLE (3).

Animal models provide the opportunity to monitor the pathologic evolution under defined conditions. Although numerous imaging techniques exist, diffusion-weighted imaging has evolved as the noninvasive method of choice for detecting acute lesions caused by cerebral ischemia (4, 5) and status epilepticus (6, 7). In diffusion-weighted imaging, contrast is modulated by molecular water diffusion. Factors influencing random water movement include the viscosity of the matrix, presence of reflective boundaries, and local temperature. Cellular membranes and other normal tissue barriers restrict the free movement of water. Also important is the viscosity differential between the intracellular and extracellular compartments. Together, these factors produce an environment in which diffusion is variably restricted, and the measurement technique must be crafted to distinguish apparent changes from real changes (8).

When water molecules reflect from a surface, the mean diffusion path is effectively reduced, resulting

Received July 29, 2003; accepted after revision December 30.

From the Division of Biomedical Engineering (S.E., E.J.K.) and the Department of Medical Imaging (E.J.K., A.O.), University of Saskatchewan, Saskatoon, Canada, and The Radiobiology Program (A.O.), Loma Linda University, CA.

Funding provided by Holliston and Associates Ltd (S.E.). Access to the imaging suite was provided by MRV Systems Inc, Saskatoon, Canada. Research supported by a grant from the Canadian Institute of Health Research (A.O.).

Address reprint requests to André Obenaus, PhD, Radiobiology Program, Loma Linda University, Chan Shun Pavilion, Room A1010, 11175 Campus Street, Loma Linda, CA 92354.

in an apparent decrease in diffusion. This specific effect can be detected in an experiment in which the time for diffusion is varied. This scenario might occur if pathologic processes, such as excitotoxic injury, produce neuronal swelling that decreases the extracellular space. Alternately, the injury cascade might include cell shrinkage and lysis, increasing the extracellular space and thus producing an increase in apparent diffusion due to decreased tortuosity (9). Real changes in diffusion follow the reallocation of water from a highly diffusing extracellular environment to a more restrictive diffusing intracellular environment (4, 10). The window for observing changes is important. Downstream from a neurotoxic event, proliferating glial populations may also contribute to a decrease in the apparent diffusion coefficient (ADC) by increasing intracellular tortuosity and thus restricting water movement (1, 11).

In this study, we explored the premise that intracellular water is restricted. If this is so, it may be possible to discriminate intracellular water from extracellular water on the basis of signal intensity on diffusion-weighted images by using a range of *b* values (4). We also hypothesized that specific isochromats are uniquely associated with evolving neuronal cell death and the subsequent gliosis, as a biologic sequel.

In our treatment, we defined diffusion isochromats as spin populations exhibiting similar mean-square diffusion paths in a fixed observation period. An extension of this treatment, termed *q space*, identifies spin populations on the basis of a probability density function belonging to an isochromat (12, 13). This investigation focused on diffusion changes in the piriform cortex at 12 hours, 24 hours, and 7 days after seizure induction. Furthermore, by observing the acute changes taking place over a range of *b* values, we could discern signatures uniquely associated with the neuronal and evolving glial populations. To our knowledge, this is the first study to use diffusion-weighted imaging to differentiate cell populations with multiple *b* values after pilocarpine-induced status epilepticus.

Methods

Animal Model

Ten male Sprague-Dawley rats (200–250 g; Charles River Laboratories, Wilmington, MA) were housed in a room with a controlled 12-hour light-dark cycle. They were allowed free access to food and water before pilocarpine injection. Animal care and use complied with institutional policies and guidelines. Freshly dissolved pilocarpine hydrochloride (380 mg/kg, intraperitoneal; Sigma, St. Louis, MO), a cholinergic agonist, was injected to induce seizures, as previously described (2, 11). Peripheral cholinergic effects were minimized by the intraperitoneal administration of scopolamine methyl nitrate (1 mg/kg; Sigma) 30 minutes before pilocarpine injection. Following pilocarpine administration, the animals were placed in an observation box, and their seizure activity was monitored. The selection process for this study involved grading seizure severity on a scale of 1 (no seizures) to 8 (repeated tonic-clonic seizures >4 hours). Ten rats with a seizure level of 4 or higher were included in the study for diffusion-weighted imaging analysis at 12 hours, 24 hours, and 7 days. At least two animals were selected for histologic analysis at each of the imaging time points.

Diffusion-Weighted Imaging

Rats were anesthetized by means of isoflurane inhalation (4% induction, 1.5% maintenance; Abbott Labs, Saint-Laurent, Quebec, Canada). Their body temperature was continuously monitored by using a rectal probe and maintained at 36°C ± 1°C by using a feedback regulatory, heated water-flow cushion. Twenty-four hours before the injection of pilocarpine, control images were obtained in each rat. Data were collected by use of a 3.0-T MR imaging unit with a 27-mm inner diameter volume quadrature coil (Morris Instruments, Ottawa, Ontario, Canada). Scout images were obtained in the coronal, transverse, and sagittal planes to accurately position the sections. Ten coronal sections, each with 2-mm thickness and interleaved by a 2-mm separation, were positioned on the sagittal scout image. These sections included the section anterior to where the hippocampus curls inferiorly. Spin-echo diffusion-weighted sequences were applied along the section (*z*) gradient (TR/TE = 3200/100). Eight *b* values (0–30,000 s/cm^2) were applied along the section axis by using a single-echo spin-echo sequence. The gradients were applied for 20 ms (δ) and the diffusion interval was set at 76 ms (Δ), but the gradient amplitude was increased at each *b* value. The field of view was 50 mm, and the matrix dimensions were 128 × 128. Two averages were used to increase the signal-to-noise ratio.

ADC maps were computed from diffusion-weighted images by using a program developed in house, as previously described (7, 14). The ADC was calculated for each pixel by using the Stejskal Tanner equation, $ADC = \ln[(S_0/S_n)/b]$, where S_n is the pixel intensity for a diffusion-weighted image and S_0 is the pixel intensity for the corresponding zero-weighted image. The calculations produced a family of maps with varying *b* values; decreased signal intensity on a diffusion-weighted map indicated a reduction in ADC.

Image Analysis

The section anterior to where the hippocampus curls inferiorly was analyzed. This position corresponded to a position at approximately −3.60 mm from bregma and represented the largest cross-sectional area for the region of interest (ROI): the piriform cortex and amygdala. The bilateral ROIs were manually drawn on the diffusion-weighted maps by using Cheshire imaging software (Hayden Image Processing Group, Waltham, MA). The piriform cortex and amygdala ROIs (both regions combined) bordered each other and extended superiorly and inferiorly. Care was taken to minimize the contribution of signal intensity from the lateral ventricles (Fig 1).

Plots of ADC versus b *Value*

ADC values were computed by using a two-point fit to the Stejskal Tanner equation and plotted against the gradient weighting (*b* value) used to obtain the map. For a homogeneous population, such a plot features a zero-slope line signifying a single population. When multiple spin populations are present, the curve features several zero-slope regions or a nonlinear negative slope, depending on the continuum of diffusing spins. We defined a diffusion isochromat as a zero-slope region on the curve of the ADC versus *b* value. Nonzero-slope components were recognized as heterogeneous populations in which the ADC changes over a specified range of *b* values.

Interpolation of Diffusion-Weighted Data

To address gradient limitations, the data were extrapolated from 30,000 (25 mT/m) to 300,000 s/cm^2 (equivalent to 85 mT/m) (13). At the same time, *b* values and data points were

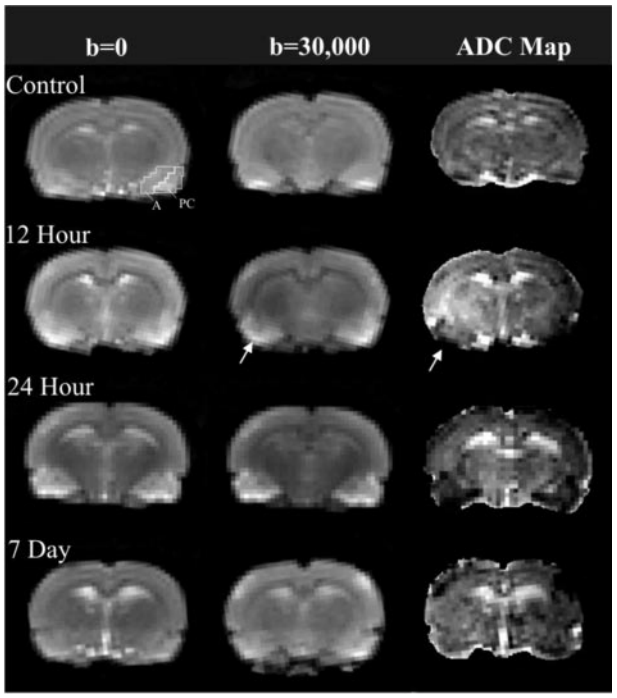

FIG 1. Spatial and temporal evolution of injury after pilocarpine-induced seizures. ROIs—piriform cortex (*PC*) and amygdala (*A*)—are defined on the first control image. Increased signal intensity in the piriform cortex and amygdala returned to control levels by 7 days. Diffusion maps were generated from unweighted (b = 0 s/cm^2) and weighted (b = 30,000 s/cm^2) images. Note increased signal intensity in the piriform cortex (*arrows*); corresponding hypointensities are seen on ADC maps, particularly at 12 hours (*arrows*).

interpolated so that a Fourier transform of ADC versus q value ($q = \gamma\delta G/2\pi$, where γ is the gyromagnetic ration, δ is the gradient amplitude, and G is the gradient duration) could be performed at uniformly spaced intervals. The data were Fourier transformed with respect to q and provided a probability distribution from which peak height and peak width at half height were extracted as measures of the relative mobility and range of mobility of the spins within the ROI (15). A more complete discussion of this approach is available (13, 16).

Statistical Analysis of MR Imaging Data

A left-versus-right comparison of ROIs was performed in all animals by using a two-tailed t test ($P < .05$). No significant differences in ADC values were found; therefore, left and right ROIs were grouped together to compare changes in ADC at each time point in a one-way analysis of variance (ANOVA) ($P < .05$). This analysis indicated that mean ADC values significantly differed among b values at each time point. A pairwise multiple-comparison procedure (Tukey test, significant at $P < .05$ and highly significant at $P < .01$) was performed to compare ADC values at individual b values for each time point to isolate differences. ADC values without significant differences for a particular time point were considered to belong to the same diffusion isochromat.

Rats were grouped to compare ADC values at different time points for a particular b value in a one-way ANOVA ($P < .05$). This analysis indicated that mean ADC values significantly differed among the time points for each b value. A pairwise multiple-comparison procedure (Tukey test, significant at $P < .05$ and highly significant at $P < .01$) was performed to compare ADCs at individual time points at the same b value in each ROI group to isolate significant differences.

Tissue Preparation and Histologic Methods

After imaging, the animals were anesthetized with a mixture of ketamine hydrochloride (126 mg/kg, intraperitoneal; Ayerst, Guelph, Ontario, Canada) and xylazine (10 mg/kg, intraperitoneal; Bayer, Etobicoke, Ontario, Canada) then euthanized. They were intracardially perfused with a fixative solution of 4% paraformaldehyde in 0.12 mol/L Millonigs phosphate buffer (1 mL/g of body weight, pH 7.3). After perfusion, brains were left in situ for 1 hour at 4°C and then postfixed for 1 hour in 4% paraformaldehyde in 0.12 mol/L Millonigs phosphate buffer. This step was followed by three 30-minute washes in 0.12 mol/L Millonigs phosphate buffer. The brains were then placed in a 20% sucrose solution for a minimum of 2 days. After the cerebellum and frontal cortex were removed, the brains were frozen over dry ice and stored at −80°C. Sections (30 μm) were obtained from brains sectioned at −20°C on a cryostat.

Sections were mounted on gelatin-chrome-alum coated slides. Cresyl violet acetate 0.5% stain (Nissl stain) was used to determine the presence of cell damage. Every 10th section was stained and included the extent of the hippocampal formation in a rostral-to-caudal direction. Sections at similar levels of the brain were also stained by means of silver nitrate impregnation, to provide a more obvious indicator of cells in the process of degeneration; this method stains dying neurons black or brown (17).

Results

Imaging Analysis

Our data (Fig 1) confirmed a temporal evolution of injury in the piriform cortex following seizures, as previously reported (7). Hyperintensities on the diffusion-weighted images rapidly appeared in the piriform cortex and evolved over 48 hours after the induction of status epilepticus. These alterations were confirmed on the ADC maps as hypointense regions, indicating substantially decreased diffusion (Fig 1). The diffusion alterations in the piriform cortex appeared to return to control levels within 7 days. Because the earliest diffusion changes were noted in the piriform cortex, this region was selected for more thorough analysis.

Our approach was to apply multiple b values spanning a range (0–30,000 s/cm^2) that could differentiate mobile populations from restricted water populations. Figure 2 shows a sample dataset of our findings, and Figure 3 provides a summary plot of our ADC results. Progressive increases in b values resulted in regional changes in signal intensity (Fig 2).

An operational definition was implemented to identify a diffusion isochromat as a horizontal region on the curve of ADC versus b when a two-point fit was used to generate the curve. With this definition, distinct diffusion isochromats were detected in the rat piriform cortex. Two spin isochromats were observed in the control piriform cortex (b = 7555–16,000 and 20,000–30,000 s/cm^2) (Fig 3). Progressive increases in b values resulted in localized changes in signal intensity (Fig 2). These signal intensity changes were plotted as a function of b value (Fig 3, *dotted lines*). Statistical analysis confirmed that these spin populations (ADC values of $[126 \pm 2.39]10^{-7}$ cm^2/s and $[108.41 \pm 2.12]10^{-7}$ cm^2/s) differed significantly at the 95% confidence interval. (The regions for lower b

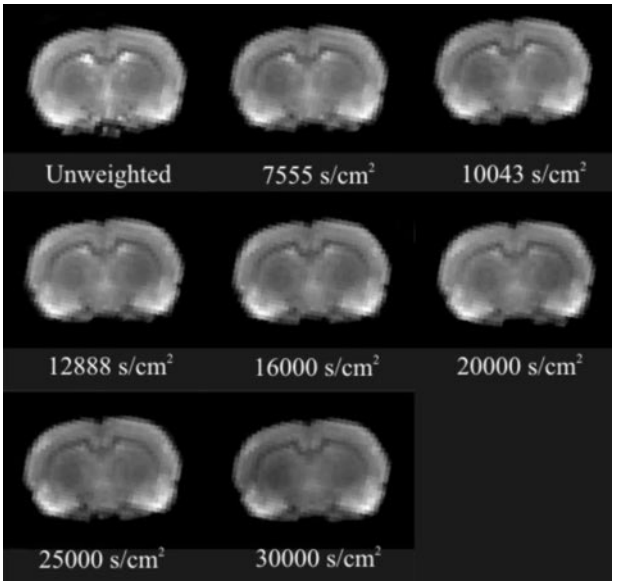

FIG 2. Typical results from a pilocarpine-treated animal at 12 hours after seizure induction illustrate the incremental contrast changes associated with increasing diffusion weighting (*b* value) during the evolution of injury. Note the decrease in signal intensity with increased *b*-value weighting.

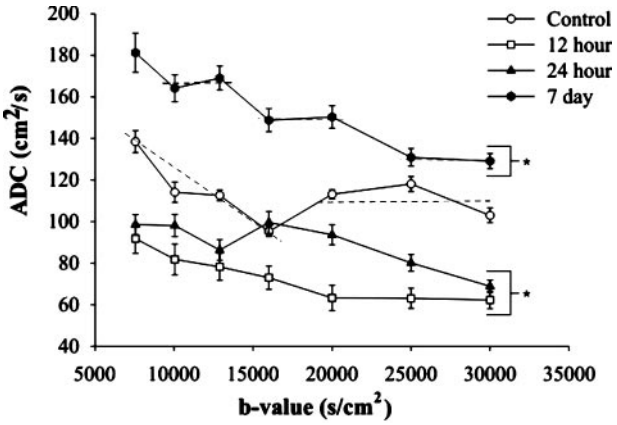

FIG 3. Plot of ADC versus *b* value in the rat piriform cortex-amygdala complex after pilocarpine-induced seizures. An isochromatic population features contiguous ADC values that fall on a horizontal line. *Dotted line* on the control plot illustrates the two isochromats in control animals. The line for low *b* value (nonzero slope) likely represents a heterogeneous cellular population, whereas the zero-slope line is likely composed of a more homogeneous cellular population. After seizures, ADC decreases, and control isochromats realign (12 and 24 hours). At 7 days, an additional isochromat emerges; this may reflect the histologically evident gliosis in the piriform cortex.

values are nonhorizontal and might be indicative of a heterogeneous cellular population or tissue matrix.)

After status epilepticus, the rats had highly significant decreases ($P < .01$) in ADC in the piriform cortex (Figs 2 and 3) at 12 hours. Two significantly different diffusion isochromats were observed at 12 hours (b = 7555–16,000 and 20,000–30,000 s/cm^2) (Fig 3). Average ADC values were (81.2 ± 5.99) × 10^{-7} cm^2/s and (62.9 ± 4.04) × 10^{-7} cm^2/s, respectively. The diffusion isochromats detected with the lowest weightings (<16,000 s/cm^2) had an average ADC decrease of 36%, whereas those detected with the higher weightings (>16,000 s/cm^2) decreased by 42% compared with control values.

Twenty-four hours after seizure induction, increased signal intensity was still observed in the piriform cortex (Fig 2), and the mean ADC remained significantly below control values, except at b = 16,000 s/cm^2 (Fig 3). Two isochromats were observed at 24 hours (b value = 7555–12,888 and 16,000–30,000 s/cm^2; $P < .05$) (Fig 3). The average ADC was 94.32 ± 3.31 cm^2/s (75% of control) and 85.56 ± 3.29 cm^2/s (79% of control).

The diffusing water populations continued to evolve for at least 7 days. The piriform cortex was hypointense relative to the control (Fig 1). At this time point, there were three significantly ($P < .05$) different diffusion isochromats (b = 7555–12,888, b = 16,000–20,000, and b = 25,000–30,000 s/cm^2). These exhibited average ADCs of 171.51 ± 5.24 cm^2/s (36% increase), 145.58 ± 3.15 cm^2/s (146% increase), and 130.02 ± 2.28 cm^2/s (20% increase), respectively (Fig 3).

In summary, the control piriform cortex ROI exhibited two isochromats on the plot of ADC versus b value (Fig 3). At 12 hours, a new, relatively immobile isochromat emerged (between 20,000 and 30,000 s/cm^2) and partially resolved by 24 hours. By 7 days, dramatic shifts in experimentally defined isochromat populations were evident, with a third isochromat emerging.

q-Space Interpolation

These studies were extended to determine if approximating the conditions for q-space acquisition might provide an additional quantitative measure of these changes. Our multiple b-value datasets clearly violated the principles of q-space imaging, but work by numerous authors has shown that interpolation of the dataset to approximate high b values can provide physiologic and diagnostic information (15, 18). After interpolating our ADC-versus-q ($q = \gamma\delta G/2\pi$) transforms, we obtained probability profiles from which full-width-at-half-maximum values (Fig 4A) provided an estimate of the mean free diffusion distance. In the control animals, mean free diffusion distances were close to 11.9 μm. This decreased to 11.5 μm by 12 hours and remained reduced at 24 hours, with a return to control levels at 7 days. Similarly, the probability of restricted (zero) displacement was dramatically reduced (82% decrease) at 12 hours; this coincided with a decrease in the mean free diffusion distance. At 24 hours, there was a subsequent increase in the probability of zero displacement, followed by a decrease at 7 days to a reduced level compared with that of control levels (42% decrease). The reduced probability-of-zero displacement in animals with seizures was reflected in a loss of isochromats exhibiting limited diffusion (Fig 4B).

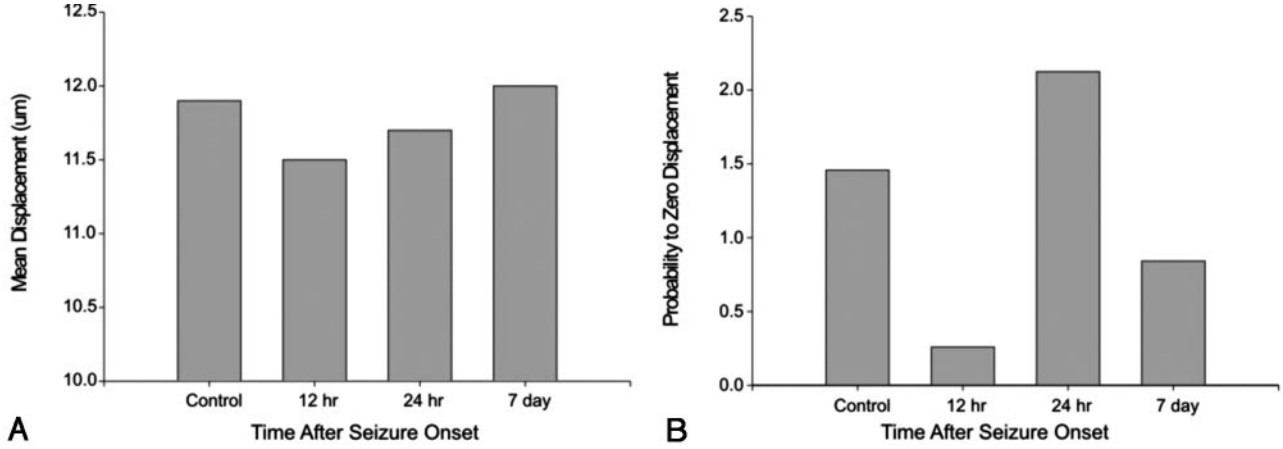

FIG 4. Extrapolation from our dataset to high *b* values yielded mean displacement and probability of zero-displacement plots.

A, Plot shows the transient decrease in mean proton displacement after seizure-induced injury. A moderate decrease is evident in the mean diffusion distance that returns to control levels by 7 days.

B, Similarly, the probability of a proton having zero displacement after seizure induction rapidly and markedly decreases at 12 hours. By 24 hours, this rebounds, indicating transient changes in the tissue matrix in the piriform cortex. By 7 days, the probability of zero displacement is reduced compared with that in control animals. Together, these extrapolation parameters support tissue remodeling that occurs as result of seizure-induced lesions.

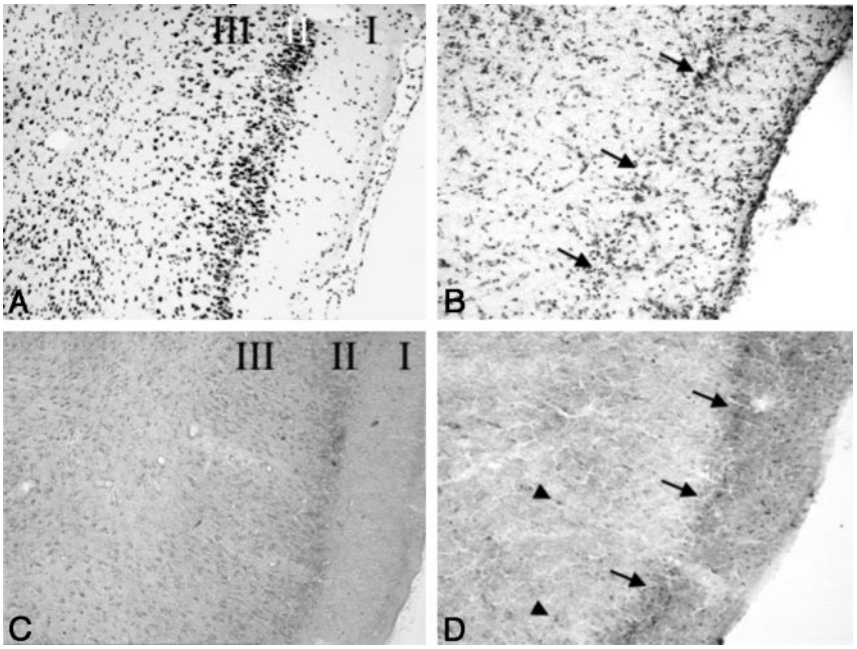

FIG 5. Cresyl violet (*A* and *B*) and silver impregnation (*C* and *D*) stains of the piriform cortex (magnification ×10).

A, Sections in a control rat after imaging shows no loss of neurons. Note the density of darkly stained neuronal nuclei in layers II and III.

B, Seven days after the induction of seizures, marked neuronal loss and vacuolization of layers II and III are seen. Note the decreased neuronal density of layer II (*arrows*).

C, Section in a control animal confirms the lack of neuronal loss.

D, Few argyrophilically stained neurons (*arrowheads*) are visible deep in the piriform cortex 7 days after seizure induction, because most degeneration took place earlier. Note the loss of neurons in layer II (*arrows*) and vacuolization of layer III.

Histologic Analysis

Tissue was processed after the final imaging time point at 7 days for histologic evaluation. Cresyl violet staining of coronal sections in tissue from control animals ($n = 3$) revealed a dense band of pyramidal cells in layer II of the piriform cortex (Fig 5A). Layer III also contained numerous healthy neurons (Fig 5A).

However, at 7 days after pilocarpine-induced seizures, the pyramidal cell layer (layer II) of the piriform cortex had been completely obliterated (Fig 5B). A similar but less dramatic reduction was also seen in layer III (Fig 5B).

Aggregations of darkly stained neurons were observed in the amygdala on cresyl violet stains. These corresponded to the neuronal nuclei of this region. Following pilocarpine administration, the amygdala contained pyknotic cells with shrunken nuclei and no nucleoli by 7 days (data not shown).

The silver-degeneration technique was used to impregnate neurons in the process of cellular degeneration; these appear as darkly stained (black or brown) cells. Control tissue lacked darkly stained cells (Fig 5C). The silver-degeneration stain confirmed the histologic features on cresyl violet stains. By 7 days, the piriform cortex exhibited neuronal loss predominantly in layers II and III (Fig 5D). Furthermore, these layers appeared largely vacuolated, as staining intensity dramatically decreased (Fig 5D).

Control tissue from the amygdala also lacked silver-stained cells. By 7 days, scattered impregnated neurons were found within amygdaloid nuclei after silver-degeneration staining (data not shown).

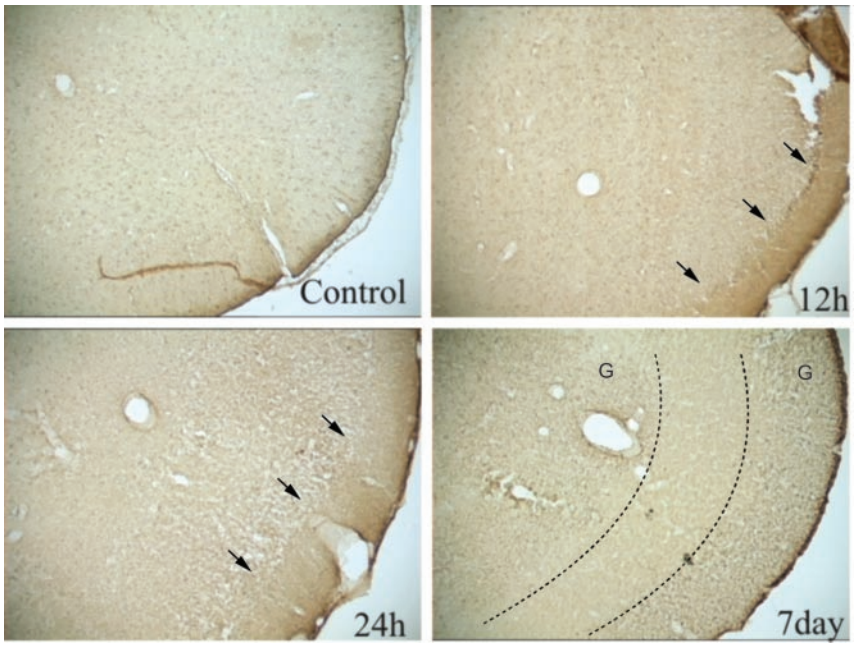

FIG 6. GFAP-stained sections of the piriform cortex-amygdala complex.

A, Control section reveals a uniform and diffuse staining pattern.

B, At 12 hours, section shows increased staining properties, particularly at the intersection of layer I and II (*arrows*).

C, This staining pattern was exacerbated at 24 hours, with increased vacuolization in layers II–IV (*arrows*).

D, Seven days after seizures, GFAP staining is substantially increased in layers I, II and IV. However, layer III (region bounded by *dotted lines*) is virtually devoid of GFAP staining but stains with OX42, an immunologic stain for microglia (data not shown). *G* indicates gliosis.

Assessment of glial reactivity to injury was performed by using glial fibrillary acidic protein (GFAP) immunohistochemistry. In control piriform cortices, uniform staining of glial cells was evident on the GFAP-stained sections (Fig 6). GFAP staining suggested few widely scattered glial cells (Fig 6A). Twelve hours after seizures, loss of staining intensity in the inner layers was evident; no significant change in glial cell staining was observed (Fig 6B). Twenty-four hours after seizures, the high-staining-intensity region in layer I broadened, and further loss of staining intensity in layers II and III were noted; an increase in glial cell staining was observed (Fig 6C). Seven days after seizures, layer I was still present, but layers II and III were represented as a featureless, medium-staining-intensity region with significantly increased glial cell staining. The area was virtually devoid of neurons (Figs 5D and 6D).

Discussion

Pilocarpine-induced status epilepticus elicits acute-onset seizures lasting for several hours, a quiescent period characterized by normalization of EEG patterns lasting for days, and subsequent spontaneous recurrent seizures lasting for weeks, similar to events in humans with TLE (2). Histopathologic features of this model demonstrate large-scale neuronal loss in the piriform cortex and amygdala, followed by upregulation of astrocytic protein markers (7, 19).

Several characteristics account for the sensitivity of the piriform cortex and amygdala to pilocarpine-induced seizures: neurons of the piriform cortex have electrical properties that allow for rapid depolarization and cell firing; in vitro electrophysiologic studies of the piriform cortex have demonstrated neuronal foci with a high predisposition to epileptiform discharges (20); in response to kindling, the amygdala demonstrates one of the lowest seizure thresholds (21); the olfactory bulbs project extensive cholinergic fibers into the amygdala and piriform cortex; and if the olfactory bulbs are removed, the administration of pilocarpine results in none of the neuropathologic damage normally associated with seizures (22).

In this study, we examined the hypothesis that diffusion-weighted imaging can differentiate presumptive cell populations after sustained seizures in the rat brain. We made several observations: 1) a decrease in ADC in the piriform cortex and amygdala at 24 hours, followed by a large increase in ADC at 7 days; 2) altered diffusion isochromats following seizures; and 3) supporting histologic features that demonstrated tissue remodeling. Together, these results support the hypothesis that *q*-space imaging can be used to discern diffusion signatures unique to neuronal and evolving glial populations.

We believe that an approximation of the *q*-space experiment is a valid method for extracting physiologic information about evolving lesions after seizures. Our physiologic findings in the piriform cortex were that the *q*-space approximation provided a semiquantitative measure of changes in the distribution of diffusion isochromats. The restricted diffusion component and the mean distance traveled are indicators of the distance between reflective boundaries. These data are well correlated with our understanding of the cellular changes that follow status epilepticus in the piriform cortex (7).

Instantaneous diffusion is an isotropic event. However, measurement constraints and the heterogeneous matrix of biologic tissues constrain water diffusion. Therefore, at the practical level, the diffusion of water in biologic systems is an anisotropic phenomenon. Because these anisotropic features are spatially selective, unique spin isochromats may serve as useful reporters of their compartmental viscosity and the

presence of reflective boundaries. In addition, because the signal-to-noise ratio is not infinite at higher *b* values with which slower diffusing spins are preferentially sampled faster, diffusing spins may become part of the noise. By carefully selecting the *b*-value range, the signal intensity can be populated with varying sets of diffusion isochromats (15, 23). Here, neuropathologic inferences were corroborated by histochemical staining.

Intracellular and Extracellular Diffusion

Diffusion in the intracellular compartment tends to be slow compared with the extracellular compartment because of the high concentration of macromolecules producing molecular crowding. In addition, cytoplasmic structures may increase the tortuosity of the diffusion path up to 10-fold (24). The cytoplasm is a viscoelastic gel, the aqueous phase of which has a viscosity two to six times that of bulk water (24). The cytosolic protein concentration is 15–26% by weight (25). As a result, there are likely to be significant hydrodynamic, steric, and electrostatic interactions among dissolved proteins that could further limit water mobility (24).

Price et al (25) speculated that water ADC values are smaller in the viscous intracellular compartment than in the more fluid interstitial region. Interestingly, Duong et al (5) found no significant difference in reported ADC measured in the intracellular compartment compared with that in the extracellular compartment. They quantified ADC by using the compartment-specific marker 2-[^{19}F]fluoro-2-deoxyglucose-6-phospate (2FDG-6P) in healthy and globally ischemic rat brains (5). Their observation, however, does not concur with our findings. If diffusion is the same in both compartments, we should not observe distinct spin populations on the plots of ADC versus *b* value. This discrepancy might result from the inherent sampling range of 2FDG-6P that corresponds to the slow diffusing water population. Indeed, many clinical systems require custom high-amplitude diffusion gradients to adequately sample 2FDG-6P diffusion.

However, seizure-induced lesions may have an etiology different from that of ischemia-induced lesions (5, 26). Seizures do not cause cessation of perfusion, energy depletion, or a change in tissue temperature that might partly account for the ADC decreases observed in ischemia (27). In addition, energy production is not arrested during seizures, although energy consumption increases enormously. Our observed decrease in diffusion after seizures (<24 hours) might suggest that intracellular viscosity increases. This is unlikely, as this early change results in cell swelling, which would require a shift of water from the extracellular compartment to the intracellular compartment. If no other intracellular change occurs, decreased viscosity results and ADC increases. Nevertheless, a decrease in viscosity involving different mechanisms due to cell death remains a possibility. The exact mechanisms that contribute to decreased ADC in vivo remain obscure.

In the piriform cortex and amygdala of the control rodent, at least two distinct spin populations of unknown origin were apparent (Fig 3). We propose that the faster and smaller spin population is composed of molecules from the extracellular compartment (25). The viscosity in the intracellular compartment is higher because of the presence of various cytosolic structures and components; therefore, the ADC of this compartment is comparably slower.

ADC, which initially decreased in the piriform cortex and amygdala at 12 hours, continued to decrease at 24 hours (Fig 3). We previously showed that progressive neuronal degeneration takes place during the 12–24-hour period (7) and that is accompanied by glial swelling (28). These observations of the piriform cortex are similar to previously reported findings (29).

The ADC decrease in the piriform cortex at 12 and 24 hours can be explained by cellular swelling in which water rapidly shifts from the extracellular into the intracellular environment (30). This is the result of neurons in this region responding to the seizure-induced excitotoxic damage. Again, with the onset of cell swelling, the extracellular space decreases in volume-restricting diffusion.

Normally, cells contain high Na^+ (140 mmol/L) and low K^+ (5 mmol/L) extracellular concentrations and low Na^+ (12 mmol/L) and high K^+ (150 mmol/L) intracellular concentrations. However, during status epilepticus, Na^+/K^+ ATPase activity increases, leading to a large increase (≈250%) in the rate of energy use, along with increased membrane ion permeability (31). When these conditions persist, ion homeostasis cannot be restored (32). High extracellular [K^+] and intracellular [Na^+] and [Ca^+] cause an osmotic gradient resulting in cellular swelling, decreased extracellular space (>30%), and increased tortuosity (33). These cellular changes in permeability and water distribution in status epilepticus are similar to those of acute ischemia (34). It is likely that there are other contributions to the observed decrease in ADC (8, 35). Nevertheless, a decrease in the extracellular space and an increase in tortuosity remain probable contributors to the observed decrease in ADC in the extracellular compartment.

Extracellular water makes up 20% (36) of brain volume, while the intracellular water accounts for the remaining 80% (34% glial, 46% neuronal) (37). Therefore, if intracellular volume increases by 6%, extracellular volume decreases by 25% (38). This sizeable change in extracellular volume would likely contribute to decreased ADC with a relatively small increase in cell volume.

Within the presumptive intracellular compartment (the slowly diffusing component), ADC also decreased (Fig 3). Water migration cannot be invoked in this case. If the cytoplasmic environment remains similar after status epilepticus, the influx of water associated with cellular edema would tend to decrease the viscosity of the intracellular compartment, thereby increasing the ADC (39). If increased viscosity underlies the observed decrease in ADC, an alternative mechanism must be sought.

Several mechanisms for increased intracellular viscosity despite the edematous condition of the cells have been proposed (5). One possibility is microtubule dissociation after cell damage, but evidence from human (40) and mouse (41) fibroblasts shows an increase in the ADC after microtubule damage (40). Therefore, it seems unlikely that microfilament disassembly accounts for the decreased ADC seen in our study.

q-*Space Diffusion*

Few reports describe *q*-space imaging in vivo. However, the considerable work of Cohen and Assaf et al (13 15, 16, 18) has focused on white matter changes in development and disease (13, 16, 18). These investigators have shown that the extrapolation of diffusion-weighted imaging findings obtained at a low *b* value to datasets obtained with a high *b* value can provide physiologic and diagnostic capabilities (15, 42). In particular, they demonstrated that the slowly diffusing population exhibits increased mean free diffusion distance and decreased probability of zero displacement in the spinal cord of spontaneously hypertensive rats (13). These changes are consistent with axonal loss and demyelineation.

Results of our own work concur with these observations. We observed a decrease in the mean free diffusion distance at 12 hours that slowly returned to control levels for the 7-day experimental period (Fig 4A). Conversely, a reduction in the probability-of-zero displacement was also observed for the 7-day period. We believe that *q*-space imaging can provide novel diagnostic information about a new cellular population (glial) after status epilepticus–induced injury. These changes are consistent with increased neuronal swelling and induction of glial hypertrophy at 12 hours, which by 24 hours leads to massive neuronal loss in the piriform cortex. Subsequent glial invasion into the cortex results in the mean free diffusion distance and probability for zero displacements returning to near-control levels.

In the present study, we observed multiple diffusion isochromats in the piriform cortex and amygdala, whereas others have seen only a single population (5). Higher diffusion weightings tend to disproportionately conceal faster spins in the noise, enabling the relative contribution of the slower spins to increase and allowing for the appearance of a larger intracellular ADC signal intensity. By 7 days, the ADC was observed to increase above control levels, possibly pointing to loss of tissue differentiation. Using a kainic acid model, Nakasu et al (43) also observed a decrease in ADC in the piriform cortex and amygdala at 24 hours and a subsequent increase in ADC at 7 days.

Interestingly, by 7 days there appeared to be three diffusion isochromats in the piriform cortex and amygdala (Fig 3); a new intermediate population had evolved. This population might represent a transition between normal tissue structure and that in which extensive gliosis has occurred. Another possibility is that three unique diffusion isochromats now exist: possibly two cell populations (original neuronal population plus another cell population) and the extracellular population. The new diffusion population could be a new mixed cell population, a group of neurons undergoing cytotoxic death, or a cell type that was increasing in number. From the previous explanation for the progression of excitotoxic cell death in the piriform cortex and amygdala, it seems highly unlikely that a different population of neurons is undergoing cell death at this time point. The literature does report a second wave of cytotoxicity, but does not support glial cell proliferation following a large loss of neurons, as occurred here (44, 45). Therefore, at this time point, many glial cells may be present to fill in the gaps left by the degenerated cells and therefore possibly account for the appearance of the new diffusion population.

Conclusion

Putative cell populations can plausibly be differentiated by inspecting line segments on curves of ADC versus *b* value. Two notably different diffusion populations (rapidly diffusing extracellular and slowly diffusing intracellular-assigned neurons) were observed in the piriform cortex and amygdala at the control point and at 12 and 24 hours. Three substantially different diffusion populations were discerned by 7 days. While population assignment is difficult, our hypothesis can support one population assigned to the extracellular space and two to intracellular spaces (probably glial and neuronal). Finally, despite severe experimental limitations, an approximation of *q*-space imaging provided a correlative measure of gliosis after status epilepticus. Together, these results provide the basis for future work with therapeutic agents designed to prevent status epilepticus–induced neuropathologic sequelae.

Acknowledgments

The authors wish to acknowledge the assistance of Yusuf Bhagat with the imaging experiments, Brenda Bartnik with the histologic analysis, and Jennifer Hadley with the animal procedures.

References

1. Swanson TH. **The pathophysiology of human mesial temporal lobe epilepsy.** *J Clin Neurophysiol* 1995;12:2–22
2. Turski WA. **Pilocarpine-induced seizures in rodents: 17 years on.** *Pol J Pharmacol* 2000;52:63–65
3. Andrew RD, Taylor CP, Snow RW, Dudek FE. **Coupling in rat hippocampal slices: dye transfer between CA3 pyramidal cells.** *Brain Res Bull* 1982;8:211–222
4. Moseley ME, Cohen Y, Mintorovitch J, et al. **Early detection of regional cerebral ischemia in cats: comparison of diffusion- and T2-weighted MRI and spectroscopy.** *Magn Reson Med* 1990;14:330–346
5. Duong TQ, Ackerman JJH, Ying HS, Neil JJ. **Evaluation of extra- and intracellular apparent diffusion in normal and globally ischemic rat brain via ^{19}F NMR.** *Magn Reson Med* 1999;40:1–13
6. Sheardown MJ, Nielsen EO, Hansen AJ, Jacobsen P, Honore T. **2,3-dihydroxy-6-nitro-7-sulfamoyl-benzo(F)quinoxaline: a neuroprotectant for cerebral ischemia.** *Science* 1990;247:571–574
7. Wall CJ, Kendall E, Obenaus A. **Rapid alterations in diffusion-**

weighted images with anatomical correlates in a rodent model of status epilepticus. *AJNR Am J Neuroradiol* 2000;21:1841–1852
8. Thomas DL, Lythgoe MF, Pell GS, Calamante F, Ordidge RJ. **The measurement of diffusion and perfusion in biological systems using magnetic resonance imaging.** *Phys Med Biol* 2000;45:R97–R138
9. McCabe RT, Wamsley JK, Yezuita JP, Olsen RW. **A novel GABAA antagonist [3H]SR 95531: microscopic analysis of binding in the rat brain and allosteric modulation by several benzodiazepine and barbiturate receptor ligands.** *Synapse* 1988;2:163–173
10. van der Toorn A, Sykova E, Dijkhuizen RM, et al. **Dynamic changes in water ADC, energy metabolism, extracellular space volume, and tortuosity in neonatal rat brain during global ischemia.** *Magn Reson Med* 1996;36:52–60
11. Obenaus A, Esclapez M, Houser CR. **Loss of glutamate decarboxylase mRNA-containing neurons in the rat of the dentate gyrus following pilocarpine-induced seizures.** *J Neurosci* 1993;13:4470–4485
12. Callaghan PT. **Principles of nuclear magnetic resonance microscopy.** Oxford: Clarendon Press; 1991:371–419
13. Cohen Y, Assaf Y. **High b-value q-space analyzed diffusion-weighted MRS and MRI in neuronal tissues - a technical review.** *NMR Biomed* 2002;15:516–542
14. Bhagat YA, Obenaus A, Hamilton MG, Kendall EJ. **Magnetic resonance imaging predicts neuropathology from soman-mediated seizures in the rodent.** *NeuroReport* 2001;12:1481–1487
15. Assaf Y, Cohen Y. **Assignment of the water slow-diffusing component in the central nervous system using q-space diffusion MRS: implications for fiber tract imaging.** *Magn Reson Med* 2000;43:191–199
16. Assaf Y, Mayk A, Cohen Y. **Displacement imaging of the spinal cord using q-space diffusion-weighted MRI.** *Magn Reson Med* 2000;44:713–722
17. Nadler JV, Evenson DA. **Use of excitatory amino acids to make axon-sparing lesions of hypothalamus.** *Methods Enzymol* 1983;103:393–400
18. Assaf Y, Holokovsky A, Berman E, Shapira Y, Shohami E, Cohen Y. **Diffusion and perfusion magnetic resonance imaging following closed head injury in rats.** *J Neurotrauma* 1999;16:1165–1176
19. Obenaus A, Houser CR. **Neuronal degeneration in the pilocarpine model of chronic seizures: Differential vulnerability and time course.** *Epilepsia* 1992;33:36
20. Haberly LB, Sutula TP. **Neuronal processes that underlie expression of kindled epileptiform events in the piriform cortex *in vivo*.** *J Neurosci* 1992;12:2211–2224
21. Goddard G, McIntyre D, Leech C. **A permanent change in brain function resulting from daily electrical stimulation.** *Exp Neurol* 1969;25:295–330
22. Millan M, Patel S, Meldrum B. **Olfactory bulbectomy protects against pilocarpine-induced motor limbic seizures in rats.** *Brain Res* 1986;398:204–206
23. Callaghan P. **Structural imaging using q-space.** *In: Principles of Nuclear Magnetic Resonance Microscopy.* Oxford: Oxford University Press, 1995:371–419
24. Luby-Phelps K, Lanni F, Taylor D. **The submicroscopic properties of cytoplasm as a determinant of cellular function.** *Ann Rev Biophys Biophys Chem* 1988;74:2259–2271
25. Price WP, Barzykin AV, Hayamizu K, Tachiya M**. A model for diffusive transport through a spherical interface probed by pulsed-field gradient NMR.** *Biophysics J* 1998;74:5
26. Charriaut-Marlangue C, Aggoun-Zouaoui D, Represa A, Ben-Ari Y. **Apoptiotic features of selective neuronal death in ischemia, epilepsy and gp120 toxicity.** *Trends in Neuroscience* 1996;19:109–114
27. Auer RN, Siesjo BK. **Biological differences between ischemia, hypoglycemia, and epilepsy.** *Ann Neurol* 1988;24:699–707
28. Olney JW, Fuller TA, deGubareff T. **Acute dendrotoxic changes in the hippocampus of kainate treated rats.** *Brain Res* 1979;76:91–100
29. Turski WA, Cavalheiro EA, Schwarz M, Czuczwar SJ, Kleinrok Z, Turski L. **Limbic seizures produced by pilocarpine in rats: a behavioural, electroencephalographic and neuropathological study.** *Behav Brain Res* 1983;9:315–336
30. Pierpaoli C, Righini A, Linfante I, Tao-Cheng JH, Alger JR, Di Chiro G. **Histopathologic correlates of abnormal water diffusion in cerebral ischemia: diffusion-weighted MR imaging and light and electron microscopic study.** *Radiology* 1993;189:439–448
31. McNamara JO. **Cellular and molecular basis for epilepsy.** *J Neurosci* 1994;3413–3425
32. Helpern JA, Huang N. **Diffusion-weighted imaging in epilepsy.** *Magn Reson Imaging* 1995;13:1227–1231
33. Lansberg MG, O'Brien MW, Norbash AM, Moseley ME, Morrell M, Albers G. **MRI abnormalities associated with partial status epilepticus.** *Neurology* 1999;52:1021–1027
34. Flacke S, Wüllner U, Keller E, Hamzei F, Urbach H. **Reversible changes in echo planar perfusion- and diffusion-weighted MRI in status epilepticus.** *Neuroradiology* 2000;42:92–95
35. Zhong J, Petroff OAC, Prichard JW, Gore JC. **Changes in water diffusion and relaxation properties of rat cerebrum during status epilepticus.** *Magn Reson Med* 1993;30:241–246
36. Nicholson C REM. **The migration of substances in the neuronal microenvironment.** *Ann NY Acad Sci* 1986;481:45–68
37. Black JA, Waxman S, Ransom BR, Feliciano MD. **A quantitative study of developing axons and glia following altered gliogenesis in rat optic nerve.** *Brain Res* 1986;380:122–135
38. Anderson AW, Zhong J, Petroff OAC, et al. **Effects of osmotically driven cell volume changes on diffusion-weighted imaging of the rat optic nerve.** *Magn Reson Med* 1996;35:162–167
39. Wick M, Nagatomo Y, Prielmeier F, Frahm J. **Alteration of intracellular metabolite diffusion in rat brain in vivo during ischemia and reperfusion.** *Stroke* 1995;26:1930–1934
40. Wojcieszyn JW, Schlegel RA, Wu ES, Jacobson KA. **Diffusion of injected macromolecules within the cytoplasm of living cells.** *Proc Natl Acad Sci U S A* 1981;78:4407–4410
41. Mastro AM, Babich MA, Taylor WD, Keith AD. **Diffusion of a small molecule in cytoplasm of mammalian cells.** *Proc Natl Acad Sci U S A* 1984;81:3414–3418
42. King MD, Houseman J, Roussel SA, Van Bruggen N, Williams SR, Gadian DG. **q-Space imaging of the brain.** *Magn Reson Med* 1994;32:707–713
43. Nakasu Y, Nakasu S, Morikawa S, Uemura S, Inubushi T, Handa J **Diffusion-weighted MR in experimental sustained seizures elicited with kainic acid.** *AJNR Am J Neuroradiol* 1995;16:1185–1192
44. Hudson LP, Munoz DG, Miller L, McLachlan RS, Girvin JP, Blume WT. **Amygdaloid sclerosis in temporal lobe epilepsy.** *Ann Neurol* 1993;33:622–631
45. Sykova E, Chvatal A. **Extracellular ionic and volume changes: the role in glia-neuron interaction.** *J Chem Neuroanat* 1993;6:247–260